RHODAMINE-B DYE PHOTODEGRADATION ON Fe-DOPED TiO_2 NANOPARTICLES SYNTHESIZED BY FLAME SPRAY PYROLYSIS

Mohamed A. Ismail[1], Nasir K. Memo[2], Mohamed N. Hedhili[3], Dalaver H. Anjum[3],Manas Bhunia[4],and Suk Ho Chung[1]*

[1]Clean Combustion Research Center (CCRC), King Abdullah University of Science and Technology (KAUST), Thuwal, Saudi Arabia E-mail; : mohamed.ismail@kaust.edu.sa
[2]Qatar Environment and Energy Research Institute (QEERI), HBKU, Qatar Foundation, Doha, Qatar
[3]Imaging and Characterization Lab, KAUST, Thuwal, Saudi Arabia
[4]KAUST Catalysis Center, KAUST, Thuwal, Saudi Arabia

ABSTRACT

Fe-doped TiO_2 nanoparticles, with varied iron to titanium atomic ratio from 0 to 10% were synthesized by flame spray pyrolysis (FSP) process, and were used as a photocatalyst for waste water management (Rhodamine B dye degradation). Particle morphology, phase formation, and elemental structure were studied using XRD, Raman, ICP-OES, BET, TEM/HRTEM, EDS, and XPS. For pure TiO_2 nanoparticles (~20 nm), anatase was the dominate phase, while iron doping promoted the formation of the rutile phase. EDS, and HRTEM confirmed that iron was uniformly doped within TiO_2. A mixture of Fe^{2+} and Fe^{3+} was observed for the samples, where at lower iron concentration Fe^{2+} was common, while Fe^{3+} was dominant at higher iron concentration. The band gap for Fe-doped TiO_2 was shifted lower by ~1eV when compared to pure TiO_2 and UV-vis confirmed the increased absorption in the visible light region. Finally, the photocatalytic activity of the prepared nanoparticles was assessed by the photo-degradation of organic pollutants under visible-light irradiation. Rhodamine B (Rh-B) was used as a model organic pollutant found in waste water containing dye. The results indicated that Fe-doping enhanced the photo-reactivity of the TiO_2 nanoparticles with the highest degradation efficiency obtained at 10% Fe in TiO_2.

Keywords: Waste water treatment, Nanoparticles, Flame Synthesis, Doped-TiO_2

1 INTRODUCTION

Photocatalysis has sparked worldwide interestfor future applications related to environmental cleaning and energy regeneration (Linsebigler et al., 1995, Lindan et al., 1996, Nie et al., 2009). TiO_2-based photocatalysts have been involved in many recent studies due to their low cost, easy preparation, high stability, and nontoxicity(Fujishima et al., 2000, Hoffmann et al., 1995). TiO_2 has a large band gap (3.0 ~3.2 eV) and thus only could be activated under UV light which is less than 5% of the solar light. Besides, TiO_2 exhibits easy recombination between holes and photoelectrons (h^+, e^-) which lowers its quantum yield. Transition metal doping of TiO_2 is a very promising way to decrease the band gap and reduce the e^-/h^+ recombination and consequently to extend light absorption to the visible region (Zhu et al., 2007, Li et al., 2003, Yu et al., 2005).Iron-ions are frequently employed as dopant to TiO_2 nanoparticles owing to their ability to reduce the band gap and reduce the e^-/h^+ recombination through selective capturing of photoelectrons (Choi et al., 1994, Wang et al., 2000, Li et al., 2003). Fe-doped TiO_2 also exhibited enhanced activity under visible-light irradiation for the degradation of water pollutants such as; methylene blue (MB) (Zhu et al., 2007), methanol (Wang et al., 2000), methylene orange (MO) (Zhang and Lei, 2008), toluene (Butler and Davis, 1993), and Rhodamine B (Rh-B)(Yang et al., 2009, Aarthi and Madras, 2007, Deng et al., 2009).

Fe-doped TiO_2 nanoparticles have been synthesized using wet-chemistry based methods (Hirano et al., 2004, Zhang et al., 2003, Wang et al., 2005). Typically, a number of steps are involved in using such methods (as well as post annealing), to obtain crystallized samples. Also higher doping concentrations (Fe 3 atom%), will result in phase segregation, due to annealing (Wang et al., 2005). A key advantage of gas-phase methods is the ability to produce Fe-TiO_2 nanoparticles in a single-step process. Wang *et al*. (Wang et al., 2005), used an RF thermal plasma for the production of Fe-TiO_2 nanoparticles, with a Fe/Ti ratio ranging from 0 to 20%, where increased iron doping promoted the transformation from anatase to rutile nanoparticles. Teoh *et al.*(Teoh et al., 2007), used FSP for synthesis of Fe-TiO_2 with titanium tetraisopropoxide (TTIP), and iron naphthenate as the precursor for Ti and Fe, respectively. The Fe/Ti ratio approached 5%, five times higher than conventional wet techniques that are followed by annealing.

Ferrocene being nontoxic, air stable, and readily soluble in pure liquid hydrocarbons (Hirasawa et al., 2004) was used as the source of iron in the synthesis of Fe-doped TiO_2 nanoparticles. Ferrocene has been widely studied in the combustion community as a fuel additive for soot reduction (Hirasawa et al., 2004, Zhang and Megaridis, 1996). It has also been used as a catalyst for the growth of carbon nanotubes (Vander Wal and Hall, 2002, Kuwana and Saito, 2007), and as an additive in diffusion flames for controlling the surface area of silica nanoparticles (Fotou et al., 1995). To the best of our knowledge, the use of ferrocene has yet to be reported using FSP. In the present study, ferrocene combined with TTIP was used as the precursor for the synthesis of Fe-doped TiO_2 nanoparticles. Detailed characterization was carried out to verify the morphology, elemental composition and optical properties of the particles. Finally, the photocatalytic behavior of the generated particles was tested for the photo-degradation of Rhodamine B as one of the major pollutants found in the industrial waste water.

2 EXPERIMENTAL PROCEDURES

2.1 Catalyst Preparation

A flame spray pyrolysis (FSP) process, was implemented to synthesize TiO_2 and Fe-TiO_2 nanoparticles. A detailed description of the experimental setup could be found in our previous work (Mohamed A. Ismail, 2016). Methane (purity 99.995%) was mixed with oxygen (O_2; purity 99.9995%), for the pilot flame; whereas oxygen at 8 bar was used as the dispersion gas in the spray nozzle for precursor atomization. TTIP (Sigma-Aldrich, 97% purity), was used as the precursor for TiO_2 nanoparticles, and ferrocene (Sigma-Aldrich, 98%) dissolved in m-xylene (Sigma-Aldrich, 99%), was mixed with TTIP for Fe-TiO_2 nanoparticles. The concentration of ferrocene was varied to obtain several Fe/Ti ratios. Ferrocene was added to TTIP with various concentrations to obtain Fe-doped TiO_2 nanoparticles with 1, 3, 5, and 10 atom% of iron with respect to the molar percentage of TiO_2.The precursor was injected using a syringe pump directly into the spray nozzle. Synthesized nanoparticles were collected on a glass-fiber filter with the aid of a vacuum pump. The generated samples were denoted FT1, FT3, FT5, and FT10 according to the concentration of iron added to the precursor. The pure titania can be simply denoted as FT0 as it does not contain any iron.

2.2 Catalyst Characterization

Collected nanoparticles were characterized using X-ray diffraction (XRD), (Bruker, D8), with CuKα radiation (λ=1.5406 Å). Raman spectroscopy measurements were performed (Aramis, LabRAM HR Visible), using 473 nm excitation. The specific surface area (SSA), was calculated based on multi-point Brunauer–Emmett–Teller (BET), nitrogen adsorption (Micromeritics, ASAP 2420). Nanoparticles were characterized using X-ray photoelectron spectroscopy (XPS), for surface chemistry, ultraviolet-visible spectroscopy (UV-vis, Varian Cary 500), for light absorbance, and inductively-coupled plasma (Varian ICP-OES 720 ES), for metal traces.The primary particle size and morphology were examined by transmission electron microscope (TEM), model Titan 80-300 ST from FEI Company, by operating it at an accelerating voltage of 300 kV. The entire TEM data were

acquired and analyzed using Digital-Micrograph Software Package version GMS1.85 from Gatan, Inc.

2.3 Photocatalytic Activity Test

Photodegradation experiments were performed with a photocatalytic reactor systembased on the degradation of Rhodamine B (Rh-B) solution under visible-light irradiation. For a typical run, 40 mg of the samples was addedinto 100 mL organic pollutant solution (20 mg/L) followed by 60 min of stirring in dark, in order to reach adsorption-desorption equilibrium previous to the photodegradation experiments.The reactor was filled with 100 mL (20 mg L−1) solution of dye and 40 mg catalyst. The temperature of the whole reactor was maintained at 298 K by using cold-water circulation. Then, thesuspension was irradiated by a Xenon lamp (CX-04E) with an optical filter cutting off wavelengthsbelow 420 nm.At regular time interval, ~ 2 ml suspension was withdrawn and centrifuged at 14,000r/m for 5 min to remove the catalysts. Then, the concentrations of the dye solutions were calculated by measuring their absorbance at the maximum absorption peak of the Rhodamine B at 553 nm. The percentage of degradation is recorded as C/C_0. Here, C is the absorption of Rh-B solution at each irradiated time interval of the main peak of the adsorption spectrum, and C_0 is theabsorption of the initial concentration when the adsorption-desorption equilibrium is reached.

3 RESULTS AND DISCUSSIONS

3.1 Nanoparticle Characterization

ICP-OES was employed to accurately measure the iron percentage in the doped samples (Table 1). The amount of Fe in each sample was proportional to the amount of ferrocene added to the raw precursor and varied from 0.87 to 5.24 atom%. The SSA data using BET are also shown in Table 1. SSA for the pure TiO_2 sample was 151 m^2/g, while the surface area was reduced to 118 m^2/g for the sample FT1, after that the SSA increases monotonically with Fe ratio in the sample. Based on SSA, and assuming spherical particles, the average primary particle size $d_{BET,}$was calculated, and found to be around 10 nm for most samples.

Table1.Propertiesof the Fe-doped TiO_2 nanoparticles

Sample	Fe/Ti in precursor	Fe in doped-sample	Anatase content	d_{XRD}	SSA (BET)	d_{BET}
	%	%	%	[nm]	[m^2/g]	[nm]
FT0	0	0.0	91.8	16.2	151	9.9
FT1	1	0.87	85.8	18.8	118	12.6
FT3	3	1.56	64.2	16.3	137	10.9
FT5	5	2.61	42.1	12.2	139	10.4
FT10	10	5.24	20.9	15.9	140	10.2

XRD was used to identify the crystalline structure. Figure 1.a shows the XRD spectra, displaying peaks at $2\theta \cong 25.4$ and 27.5, which represent the anatase (101) and rutile (110) crystalline phases, respectively. The anatase phase is dominant in the pure TiO_2 nanoparticles, while iron doping reduces the anatase percentage with increased iron concentration(Li et al., 2003). The rutile phase was dominantfor the FT10 sample that contains maximum amount of iron. Anatase percentage in the samples was calculated by integrating the respective XRD peak intensities; results are listed in Table 1. Because of the similar ionic radius of Fe^{3+} and Ti^{4+}, iron can occupy the titanium position in the TiO_2 lattice. Similar results were observed in other gas-phase methods for production of Fe-TiO_2 (Wang et al., 2005, Teoh et al., 2007).

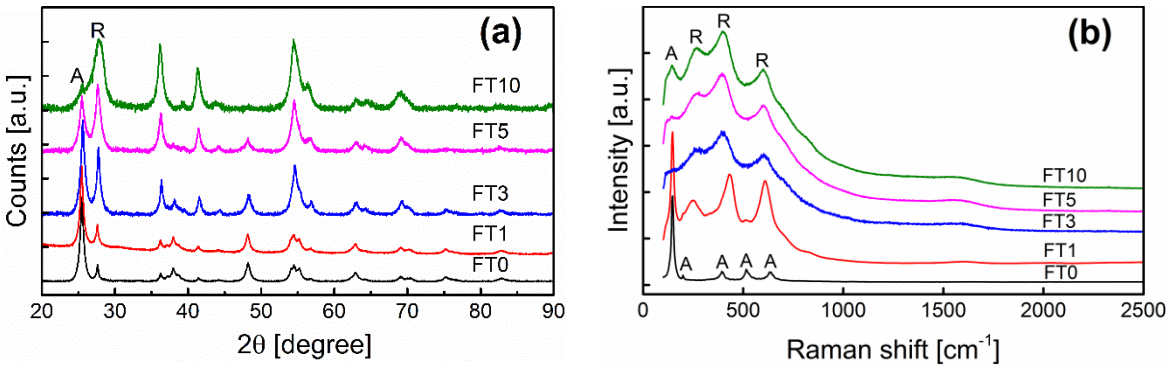

Figure 1. (a) XRD pattern and (b) Raman spectra for Fe-doped samples compared with pure TiO_2 nanoparticles. A (anatase), R (rutile)

The crystallite size d_{XRD} of TiO_2 nanoparticles was obtained from the position of the (101) and (110) peaks using the Scherrer formula, which ranged from 12-19 nm (Table 1). Raman spectroscopy was performed to further characterize the TiO_2 nanoparticles. The Raman spectra (Fig. 1.b) show that the anatase phase was dominant for the pure TiO_2 samples, while the rutile phase was dominant for the Fe-TiO_2 samples, which is consistent with previous XRD data.

TEM analysis, in conjunction with EDS, was performed to check the quality of the Fe-TiO_2 nanoparticles and their overall elemental composition. A typical electron micrograph is shown in Fig. 2a for pure TiO_2 nanoparticle, about 20 nm in size. Typical electron micrographs, acquired under HRTEM conditions, are shown in Fig.2b-d, which showhigh crystallinity and the ordered structure of the nanoparticle lattice planes for all studied samples.The particle morphology in Fe-doped cases (FT3 and FT10), is similar to that of a pure TiO_2 sample. The SAED pattern of pure TiO_2 NPs (upper-right inset of Fig. 2b) shows uniform rings due to diffraction from anatase peaks which agrees with XRD results. Diffraction pattern for FT3 and FT10 samples confirms the presence of both anatase and rutile peaks which are in a good agreement with XRD results shown previously.

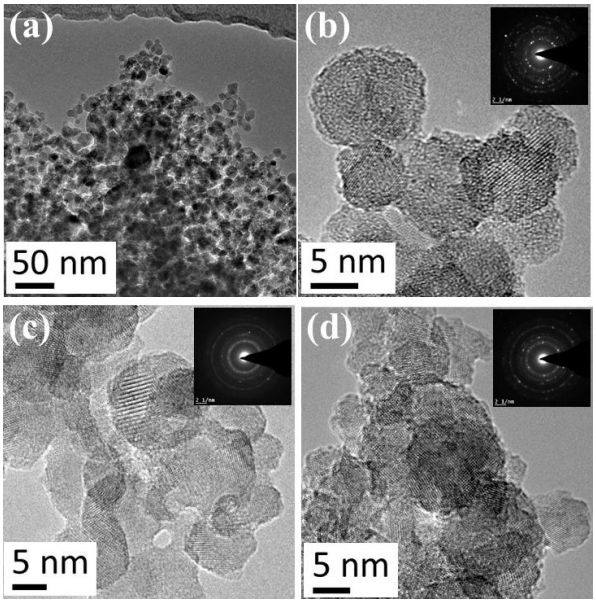

Figure 2.(a) TEM for the pure TiO_2 NPs, and HRTEM for (b) FT0, (c) FT3, and (d) FT10 samples with SAED patterns in the upper right inset.

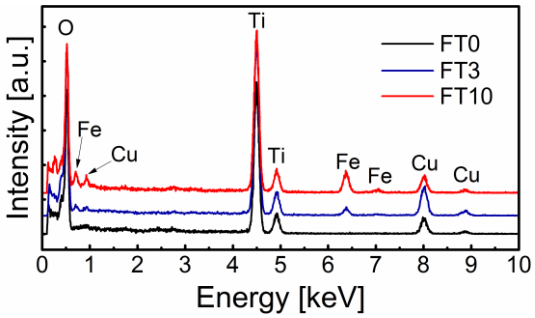

Figure 3. EDS spectra confirming the presence of iron in doped-TiO_2 samples.

EDS spectra data are shown in Fig. 3, confirming the presence of O and Ti elements in the pure TiO_2 nanoparticles. For iron-doped samples (FT3 and FT10), Fe peaks appear, which increased with increasing iron doping along with additional Fe peaks indicating higher concentration of iron in the sample. The spectrum also contains Cu peaks, attributable to the Cu-grid.

Chemical composition was analyzed using XPS. High resolution XPS spectra of the Fe 2p core level from Fe-doped TiO_2 at various iron percentages are shown in Fig. 4. The Fe 2p core level was fitted using eight. The peaks at 710.8 eV (Fe $2p_{3/2}$ doublet), and 719.4 eV (corresponding satellite peak), together with 724.3 eV (Fe $2p_{1/2}$ doublet), and 732.9 eV (corresponding satellite peak), are characteristic of the Fe^{3+} oxidation state of iron (Fujii et al., 1999, Barreca et al., 2001). Also, the satellite peaks, situated at 8.6 eV from the main peaks, are a signature of Fe^{3+} ions.The peaks at 709.1 (Fe $2p_{3/2}$ doublet), and 715.3 eV (corresponding satellite peak), together with 722.3 (Fe $2p_{1/2}$ doublet), and 728.5 eV (corresponding satellite peak), are characteristic of Fe^{2+} oxidation state of iron (Aronniemi et al., 2005, Barreca et al., 2001). Also, the satellite peaks situated at 6.2 eV from the main peaks are a signature of Fe^{2+} ions. The area ratio of Fe $2p_{3/2}$ – Fe $2p_{1/2}$ components is equal to 2:1 and the doublet separation is equal to 13.5 eV for Fe^{3+} and to 13.2 for Fe^{2+}. Increasing the percentage of the Fe dopant led to an increase of the Fe^{3+}/Fe^{2+} ratio from 0.5 for FT3 to 1.8 for FT10 samples which is preferred for photocatalytic applications (Li et al., 2003).

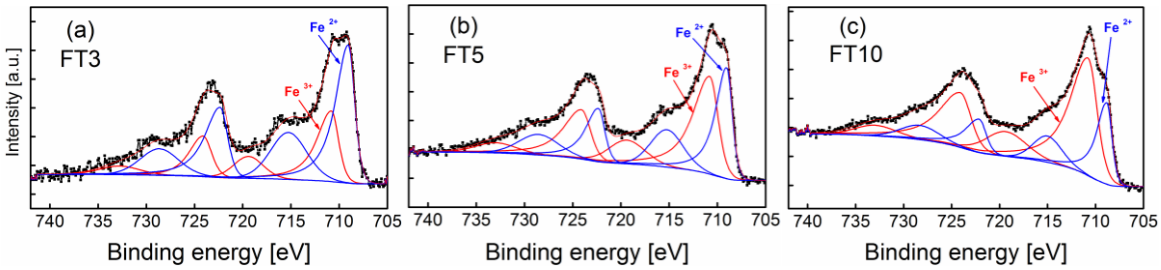

Figure 4: High resolution spectra of Fe 2p peaks for (a) FT3, (b) FT5, and (c) FT10 samples.

The UV-vis absorption spectra (Fig. 5), were used to identify light absorption from undoped and doped TiO_2 samples. Pure TiO_2 exhibited an absorption edge that rose steeply toward the UV region below 400 nm, which could be attributed to the band-gap excitation of anatase (3.2 eV), without absorption in the visible region (>400 nm) (Sun et al., 2013). Doping TiO_2 nanoparticles with iron significantly enhanced light absorption between 400 to 550 nm. The visible light absorption increased monotonically with increased iron concentration similar to other results in literature (Choi et al., 1994, Zhu et al., 2004), accompanied by the change of powder color from white to brown. This result indicates increased visible light absorption of TiO_2 nanoparticles, occurring after doping with iron.

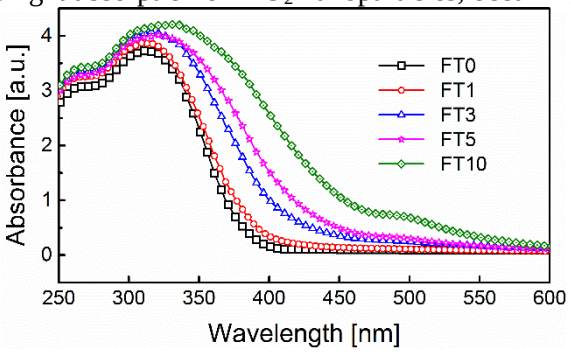

Figure 5: Ultraviolet-visible (UV-vis), spectra for pure and Fe-doped TiO_2 samples.

3.2 Degradation of Rhodamine B

After characterization of the synthesized nanoparticles, it was very clear that the optical response ofTiO_2 was shifted from UV to visible-light region with theintroduction of irondopant.The optical response was monotonically increasing with the concentration of Fe in the TiO_2 NPs. Thisimplied that these Fe-doped TiO_2 catalysts, unlike pure TiO_2,might be very active under visible-light irradiation.

Being a well-known as a major pollutant of industrial waste water we have studied the photodegradation of rhodamine B in an aqueous solution. We have shown the catalytic efficiency of the Fe-doped TiO_2nanomaterials in photodegradation of Rh-B in an environmentally benign route as shown in Fig. 6. Before the reaction,Rhodamine B/Fe-TiO_2photocatalyst mixtures are taken in a

beaker and stirred in dark for 60 min to get a homogeneous suspension. Samples have been collected within regular time intervals and monitored by UV–visible absorption spectra regarding λ_{max} at 553 nm, the characteristic absorbance wavelength of Rhodamine B. Fig. 6 clearly demonstrates that the absorbance (at λ_{max}) of thedye decreases continuously with increase of time in the presence of FT10 sample. The decolorization and degradation efficiency have been calculated by employing the following equation

$$D\% = \left[1 - \frac{C}{C_0}\right] \times 100 (1)$$

where C_0 is theinitialconcentrationofdyeand C is theconcentration ofdyeafterirradiationinselectedtimeinterval.

According to Beer's law, the absorbance at the characteristic absorbance wavelength of Rh-B (553 nm) was proportional to the concentration of the dye in the reaction solution. The concentration of Rh-B after desorption-adsorption equilibrium was assumed to be the initial concentration (C_0) to eliminate any effect of adsorption in the dark on the dye concentration and to ensure that any change in the dye concentration is only due to the chemical reaction.

Figure 7 shows the degradation rates of Rh-Bin the presence of pure TiO_2 and Fe-doped TiO_2NPs under visible-light radiation. About12% of the Rhodamine Bwas degraded in the presence of pure TiO_2NPs after 2 hours of radiation, while this value increased to 20% in the presence of FT1sample which contains less than 1 atom% of iron.As iron concentration in the titania NPs further increases, the degradation efficiency of Rh-B increased monotonically reaching to 53% in the presence of FT10 sample. The degradation efficiencies of the current samples are comparable to values in literature (Yang et al., 2009, Aarthi and Madras, 2007, Deng et al., 2009).After absorbing light, the excited dye (Rhodamine B) injected an electron into the conduction band of$TiO_2$where itwas captured bysurface-adsorbedO_2 to form$O_2^{\bullet -}$, andthen, the dye cation radicals were degraded via attack by oxygenactive species(Fu et al., 2005). In addition, itwas noticed that the degradation of Rh-B did not occur in the absenceof catalysts or visible-light under the experimental conditions.

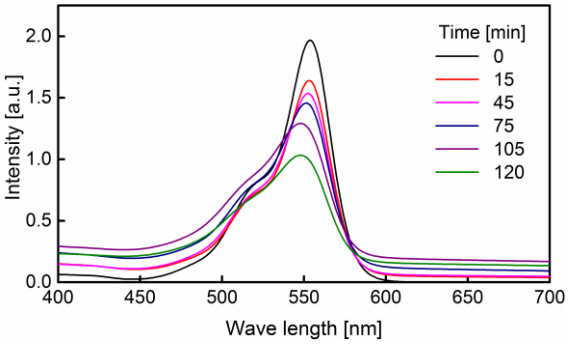

Figure 6:Decrease absorption spectra of Rhodamine B in the presence of FT10 sample at different irradiation times.

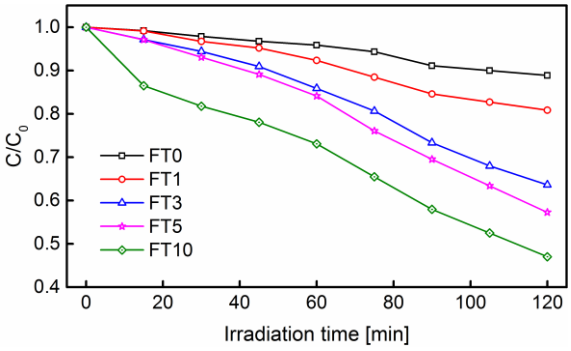

Figure 7:Plots of concentration of Rhodamine B vs irradiation time in the presence of iron-doped samples.

Thefirst-orderrateconstant k (min^{-1}) for photodegradationofdyes has been calculatedbyemploying thefollowingequation:

$$lnC = lnC_0 - kt (2)$$

where C_0 and C are dyeconcentrationsinitiallyandaftertime t, respectively. According to the above kinetic model, the rate constants (k) were found to be 0.001, 0.0019, 0.0039, 0.0047, and 0.006 min^{-1} for samples FT0, FT1, FT3, FT5, and FT10, respectively. The rate constant for the photodegradation of Rhodamine B using Fe-TiO_2 previuosly reported was 0.0029 min^{-1} and 0.00016 min^{-1} for P25 (Yang et al., 2009).Higherrateconstantsforthedecomposition ofRh-Bofour synthesizedmaterialsthanstandard P25and Fe-TiO_2 NPs prapared using different methodssuggestedthatour materialsaremoreactive.Hence,abovefindings

clearlydemonstratethathigheramountofironincorporationinto the framework of TiO_2 makes the catalyst more efficient for photocatalytic degradation of organic dyes.

4 CONCLUSIONS

In this work, we successfully prepared Fe-doped TiO_2 NPs using flame spray pyrolysis (single-step process) and ferrocene as the precursor for iron in the doped samples with particle size around 20 nm. Adding iron as a dopant changed the physical and chemical properties of TiO_2NPs. As increasing the iron concentration, the phase changes from anatase to rutile and the amount of Fe^{3+} increases. Doping TiO_2 nanoparticles with iron significantly enhanced light absorption between 400 to 550 nm (photo absorbance was extended to the visible-light region). The visible light absorption increased monotonically with increased iron concentration. It was assumed that these dopants introduced impurity levels between the conduction and valence band of TiO_2, leading to narrower band gap and enhancing the visible-light absorption. Compared with TiO_2, these catalysts showed much higher activity for the degradation of Rhodamine B under visible-light irradiation.Finally, development of cost effective photo-catalysts with proven non toxicity effects on environment could have a positive impact on water treatment in the future.

ACKNOWLEDGMENTS

This work was supported by King Abdullah University of Science and Technology (KAUST) under a CCF Grant.

REFERENCES

AARTHI, T. & MADRAS, G. 2007. Photocatalytic degradation of rhodamine dyes with nano-TiO2. Ind.Eng.Chem.Res. 46, 7-14.

ARONNIEMI, M., SAINIO, J. & LAHTINEN, J. 2005. Chemical state quantification of iron and chromium oxides using XPS: the effect of the background subtraction method. Surf. Sci. 578, 108-123.

BARRECA, D., BATTISTON, G. A., BERTO, D., GERBASI, R. & TONDELLO, E. 2001. Chemical Vapor Deposited Fe2O3 Thin Films Analyzed by XPS. Surf. Sci. Spec. 8, 240-245.

BUTLER, E. C. & DAVIS, A. P. 1993. Photocatalytic oxidation in aqueous titanium dioxide suspensions: the influence of dissolved transition metals. J. Photochem.Photobiol. A: Chem. 70, 273-283.

CHOI, W., TERMIN, A. & HOFFMANN, M. R. 1994. The Role of Metal Ion Dopants in Quantum-Sized TiO2: Correlation between Photoreactivity and Charge Carrier Recombination Dynamics. J. Phys. Chem. 98, 13669-13679.

DENG, L., WANG, S., LIU, D., ZHU, B., HUANG, W., WU, S. & ZHANG, S. 2009. Synthesis, characterization of Fe-doped TiO2 nanotubes with high photocatalytic activity. Catal. Lett. 129, 513-518.

FOTOU, G. P., SCOTT, S. J. & PRATSINIS, S. E. 1995. The role of ferrocene in flame synthesis of silica. Combust.Flame, 101, 529-538.

FU, H., PAN, C., YAO, W. & ZHU, Y. 2005. Visible-light-induced degradation of rhodamine B by nanosized Bi2WO6. J.Phys.Chem. B, 109, 22432-22439.

FUJII, T., DE GROOT, F., SAWATZKY, G., VOOGT, F., HIBMA, T. & OKADA, K. 1999. In situ XPS analysis of various iron oxide films grown by NO2-assisted molecular-beam epitaxy. Phys. Rev. B, 59, 3195.

FUJISHIMA, A., RAO, T. N. & TRYK, D. A. 2000. Titanium dioxide photocatalysis. J. Photochem. Photobiol. C: Photochem. Rev. 1, 1-21.

HIRANO, M., JOJI, T., INAGAKI, M. & IWATA, H. 2004. Direct Formation of Iron (III)- Doped Titanium Oxide (Anatase) by Thermal Hydrolysis and Its Structural Property. J. Am. Ceram. Soc. 87, 35-41.

HIRASAWA, T., SUNG, C.-J., YANG, Z., JOSHI, A. & WANG, H. 2004. Effect of ferrocene addition on sooting limits in laminar premixed ethylene–oxygen–argon flames. Combust. Flame, 139, 288-299.

HOFFMANN, M. R., MARTIN, S. T., CHOI, W. & BAHNEMANN, D. W. 1995. Environmental applications of semiconductor photocatalysis. Chem.Rev. 95, 69-96.

KUWANA, K. & SAITO, K. 2007. Modeling ferrocene reactions and iron nanoparticle formation: Application to CVD synthesis of carbon nanotubes. Proc.Combust.Instit. 31, 1857-1864.

LI, X., YUE, P.-L. & KUTAL, C. 2003. Synthesis and photocatalytic oxidation properties of iron doped titanium dioxide nanosemiconductor particles. New J.Chem. 27, 1264-1269.

LINDAN, P. J. D., HARRISON, N. M., HOLENDER, J. M. & GILLAN, M. J. 1996. First-principles molecular dynamics simulation of water dissociation on TiO2 (110). Chem. Phys. Lett. 261, 246-252.

LINSEBIGLER, A. L., LU, G. & YATES JR, J. T. 1995. Photocatalysis on TiO2 surfaces: principles, mechanisms, and selected results. Chem. Rev. 95, 735-758.

MOHAMED A. ISMAIL, N. K. M., MOHAMED N. HEDHELI, DALAVER H. ANJUM, VENKATESH SINGARAVELU, SUK HO CHUNG 2016. Flame Spray Pyrolysis of Fe-doped TiO2 using Ferrocene: Synthesis, Characterization and Properties. 36th International Symposium on Combustion. Seoul, Korea.

NIE, X., ZHUO, S., MAENG, G. & SOHLBERG, K. 2009. Doping of TiO2 Polymorphs for Altered Optical and Photocatalytic Properties. Int. J. Photoenergy, 2009.

SUN, L., LIN, J. X., WANG, L. & SONG, K. X. 2013 Preparation and characterization of Fe3+-doped TiO2/diatomite composite. App. Mech. Mater.Trans Tech Publ, 15-18.

TEOH, W. Y., AMAL, R., MÄDLER, L. & PRATSINIS, S. E. 2007. Flame sprayed visible light-active Fe-TiO2 for photomineralisation of oxalic acid. Catal. Today, 120, 203-213.

VANDER WAL, R. L. & HALL, L. J. 2002. Ferrocene as a precursor reagent for metal-catalyzed carbon nanotubes: competing effects. Combust.Flame, 130, 27-36.

WANG, C.-Y., BAHNEMANN, D. W. & DOHRMANN, J. K. 2000. A novel preparation of iron-doped TiO2 nanoparticles with enhanced photocatalytic activity. Chem. Commun. 1539-1540.

WANG, X., LI, J.-G., KAMIYAMA, H., KATADA, M., OHASHI, N., MORIYOSHI, Y. & ISHIGAKI, T. 2005. Pyrogenic iron (III)-doped TiO2 nanopowders synthesized in RF thermal plasma: phase formation, defect structure, band gap, and magnetic properties. J. Am. Chem. Soc. 127, 10982-10990.

YANG, X., CAO, C., ERICKSON, L., HOHN, K., MAGHIRANG, R. & KLABUNDE, K. 2009. Photo-catalytic degradation of Rhodamine B on C-, S-, N-, and Fe-doped TiO2 under visible-light irradiation. App. Catal. B: Env. 91, 657-662.

YU, J. C., HO, W., YU, J., YIP, H., WONG, P. K. & ZHAO, J. 2005. Efficient visible-light-induced photocatalytic disinfection on sulfur-doped nanocrystalline titania. Env.Sci.Technol. 39, 1175-1179.

ZHANG, J. & MEGARIDIS, C. M. 1996. Soot suppression by ferrocene in laminar ethylene/air nonpremixed flames. Combust. Flame, 105, 528-540.

ZHANG, X. & LEI, L. 2008. One step preparation of visible-light responsive Fe–TiO2 coating photocatalysts by MOCVD. Mater. Lett. 62, 895-897.

ZHANG, Y., EBBINGHAUS, S. G., WEIDENKAFF, A., KURZ, T., KRUG VON NIDDA, H.-A., KLAR, P. J., GÜNGERICH, M. & RELLER, A. 2003. Controlled iron-doping of macrotextured nanocrystalline titania. Chem.Mater. 15, 4028-4033.

ZHU, J., REN, J., HUO, Y., BIAN, Z. & LI, H. 2007. Nanocrystalline Fe/TiO2 visible photocatalyst with a mesoporous structure prepared via a nonhydrolytic sol-gel route. J. Phys. Chem. C, 111,

ZHU, J., ZHENG, W., HE, B., ZHANG, J. & ANPO, M. 2004. Characterization of Fe–TiO2 photocatalysts synthesized by hydrothermal method and their photocatalytic reactivity for photodegradation of XRG dye diluted in water. J. Mol. Catal. A: Chem. 216, 35-43.